ACS Catalysis

pubs.acs.org/acscatalysis Research Article

Temperature-Dependent Communication between Pt/Al_2O_3 Catalysts and Anatase TiO_2 Dilutant: the Effects of Metal Migration and Carbon Transfer on the Reverse Water−Gas Shift Reaction

Linxiao Chen, Libor Kovarik, and János Szanyi*

Cite This: https://doi.org/10.1021/acscatal.1c03133 Read Online

ACCESS | Metrics & More | Article Recommendations | Supporting Information

ABSTRACT: In heterogeneous catalysis, unexpected effects from the supposedly inert reactor dilutant are not rare but related understanding is lacking and inconsistent. Here, we report investigations of the impacts of the anatase TiO_2 dilutant on the reverse water−gas shift (rWGS) reaction over Pt/Al_2O_3 catalysts. Combining detailed kinetic data with microscopic and spectroscopic results, we demonstrate that the catalyst−dilutant communication depends on temperature. At a high temperature (400 °C), Pt migrates from Al_2O_3 to TiO_2, resulting in higher dispersion and activity, without changing reaction mechanisms. Pt migration is general to catalysts of different Pt nuclearity and various oxide dilutants. In contrast, at a low temperature (250 °C), carboxylic acids (in particular acetic acid) present in the ambient air and adsorbed on TiO_2 are transferred onto Al_2O_3 in close contact, effectively blocking the formate rWGS pathway. As a result, the rWGS can only proceed through the carboxyl pathway and hence is significantly slower. The acetate transfer affects catalysts of different Pt nuclearity and support but is unique to the anatase TiO_2 dilutant. As the acetate layer is slowly removed under H_2 or the rWGS stream, the activity recovers. This work elucidates the complicated communication between catalysts and dilutants, which has general implications in heterogeneous catalysis and resolves the inconsistency in related reports in the literature. The impacts that anatase TiO_2 dilution has on the rWGS also unveil mechanistic understanding that further confirms the two co-existing rWGS pathways.

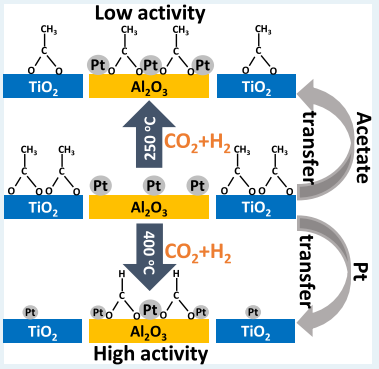

KEYWORDS: *catalyst-dilutant communication, platinum, anatase titania, metal migration, acetate, reverse water−gas shift, CO_2 hydrogenation*

1. INTRODUCTION

Reactions on the supported metal catalysts often require synergy among components. Metal−support synergy is a prominent example that has been extensively investigated.[1−4] As a result, it has been well established that the support can be more involved than being the innocent matrix to disperse the metal and regulate its structural/electronic properties.[2,5−9] Support surfaces can also participate in reactions directly through communication with the metal, in ways such as H spillover and intermediate shuttling.[4,10−12] Besides, in practice, catalysts are often diluted with another material to avoid heat and/or mass transfer concerns, which further complicates the picture.[13,14] Although the dilutant should always be inert for the reaction, in many cases, the dilutant is not as inert as it is supposed to be.[15−18] The unexpected catalyst−dilutant synergy suggests that the catalyst can also communicate with the dilutant, which could affect the reactions significantly but is not yet thoroughly explored. In addition to the fundamental interests, understanding such a phenomenon could also open novel opportunities for improving the catalytic efficiency without consuming extra noble metal.[19−22]

Literature reports regarding the catalyst−dilutant communication, despite being limited in quantity, show the complicated nature of the phenomenon. Only in hydrogenation catalysis, multiple concepts were invoked to explain divergent results. It has been proposed that H can spill over from metal sites on the catalyst to the dilutant, which rationalizes observations such as the higher rates after the dilution,[21−25] and the dilutant being active when not directly in contact with the catalyst.[17−20] Nonetheless, such claims could be myths instead of facts as alternative explanations were often neglected[16,21,26] and thermodynamically, H spillover onto irreducible supports is not likely.[10,26,27] Meanwhile, the opposite effect, that is, that the dilutant suppresses the catalytic turnover, has also been reported and attributed vaguely to carbonaceous species on the dilutant contaminating the catalyst.[16,28] Besides H and "carbon contaminants", metal can also migrate between the catalyst and the dilutant during

Received: July 12, 2021

https://doi.org/10.1021/acscatal.1c03133
ACS Catal. XXXX, XXX, XXX−XXX

reactions such as the reverse water−gas shift (rWGS), that is, CO_2 hydrogenation to CO, increasing the dispersion and reaction rate.[15,29] The diverging and often contradictory literature results indicate that multiple catalyst−dilutant communication pathways are intertwined and thus hinder their respective reliable investigations. As a result, a detailed understanding of these phenomena, for example, the identity of the "carbon contaminants", whether and how H spillover occurs, and how these migrated species impact catalysis, is difficult to acquire and hence almost non-existent.

Here, we report on the effects of anatase TiO_2 dilution on Pt/Al_2O_3-catalyzed rWGS, a reaction of both practical interest for carbon mitigation and fundamental interest for understanding hydrogenation and water−gas shift catalysis. The initial intention was to elucidate whether TiO_2 participates in the rWGS by accepting H or other intermediates, but the intended study was interfered by the observation that both Pt and adsorbed acetate on TiO_2 can move between TiO_2 and Pt/Al_2O_3, which have significant impacts on the reaction and thus demand a detailed investigation. We discovered that Pt migration requires 400 °C, increasing Pt dispersion and activity but not changing the rWGS mechanism, and occurs with a wide range of Pt species and dilutants. Acetate transfer can occur at 250 °C, deactivating Pt/Al_2O_3 by blocking the formate rWGS pathway and is mostly unique to anatase TiO_2. Details regarding the two processes and the implications on the rWGS mechanism were also studied and discussed. These results provide an intriguing understanding on the catalyst−dilutant communication, which has implications to a broad range of catalytic reactions beyond the rWGS. Besides, TiO_2 dilution offers a unique opportunity to deconvolute the two co-existing rWGS pathways, generating evidence that helps elucidate the mechanism.

2. RESULTS

2.1. rWGS at 400 °C: Pt Migration Enhancing Activity with Identical Mechanism. To investigate the catalyst−dilutant communication, 2 wt % Pt/Al_2O_3 (synthesized by incipient wetness impregnation, herein referred to as "Pt/Al_2O_3") was mixed with varying amount of anatase TiO_2 ("A-TiO_2" or "TiO_2") nanopowders ($d \approx 5$ nm, BET surface area ~ 316 m^2/g, Table S1) and ground thoroughly with a pestle to ensure close physical contact. Then, the mixture was tested for the rWGS at 400 or 250 °C under ambient pressure and compared with Pt/Al_2O_3 only. All catalysts exhibit >99% CO (rWGS) selectivity in all tests. A-TiO_2 by itself exhibits negligible activity without Pt/Al_2O_3 (Figure S1). Kinetic data at 400 °C are presented in Figure 1. Figure 1a shows that as the dilution factor, defined as the mass ratio between A-TiO_2 and Pt/Al_2O_3, increases from 0 to 10, the stabilized per-total-Pt rWGS rate (not TOF) at 400 °C (blue, Figure S2a showing the rate *vs* time-on-stream, TOS, data with an induction period of ~1 h) increases monotonously. After the rate stabilized at 400 °C, the system was cooled down to 250 °C, all samples show a stable rWGS rate (Figure S2b), and the positive correlation between the rate and the dilution factor persists (red).

To understand why TiO_2 dilution enhances the per-Pt rate, kinetic parameters of the rWGS were measured at 250 °C after the 400 °C reaction. Figure 1b shows that neither the apparent activation barrier ($E_{a,app}$, red) nor the dependence of the rate on the partial pressure of the reactants (blue for H_2 and green for CO_2), that is, reaction orders, is altered by TiO_2 dilution.

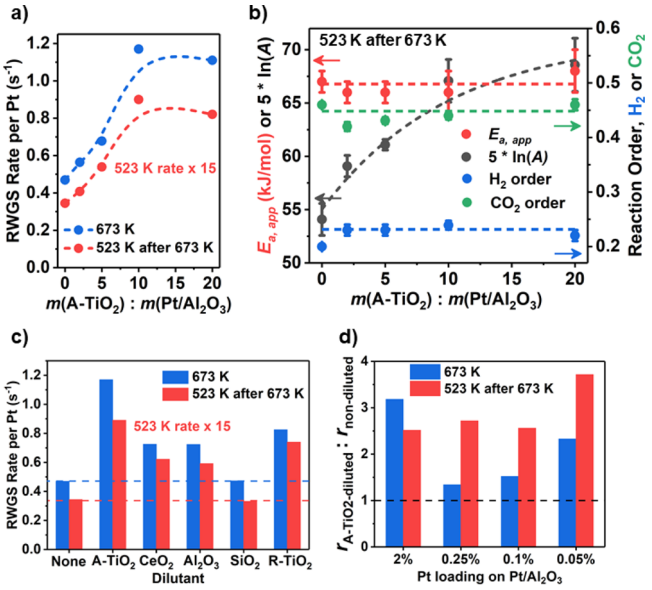

Figure 1. Kinetic data of the rWGS reaction over diluted Pt/Al_2O_3 catalysts at 400 °C (blue) and at 250 °C after cooling down from 400 °C reaction (red). Panel (a) shows the stabilized per-total-Pt rWGS rate with a varying amount of A-TiO_2 as the dilutant (rate *vs* TOS data shown in Figure S2a,b). Panel (b) summarizes kinetic parameters [red: $E_{a,app}$, blue: H_2 order, green: CO_2 order, black: the natural log of the pre-exponential factor (A) multiplied by 5] at 250 °C after 400 °C reaction, with a varying amount of A-TiO_2 as the dilutant (fitting plots shown in Figure S3). Panel (c) shows the stabilized per-total-Pt rate with various oxides of 10 times the mass of Pt/Al_2O_3 as the dilutant (rate *vs* TOS data shown in Figure S2c,d). Panel (d) shows the ratio between the rate on Pt/Al_2O_3 of various Pt loading with and without A-TiO_2 of 10 times the mass of Pt/Al_2O_3 as the dilutant, that is., the level of the rate enhancement effect due to A-TiO_2 dilution (rate *vs* TOS data shown in Figure S2e,f). Reaction conditions: 400 or 250 °C, $CO_2/H_2/He$ = 1:4:15, total flow rate = 40 sccm, $m(Pt/Al_2O_3)$ = 3 mg in the mixture, further diluted with 100 mg 70 mesh SiC.

Only the pre-exponential factor (A, black) increases with the dilution factor, implying that TiO_2 dilution does not alter the reaction mechanism. Instead, it likely increases the number of active sites, that is, Pt dispersion. Scanning transmission electron microscopy (STEM) was used to test the hypothesis. Figure 2 shows that on Pt/Al_2O_3 + A-TiO_2 used in 400 °C rWGS, small Pt clusters (d = 0.9 ± 0.2 nm, Figure 2a) were found in regions unequivocally identified as TiO_2 by energy-dispersive X-ray spectroscopy (EDX, Figure 2b). Features resembling single Pt atoms were also found in regions that are likely TiO_2 (Figure 2c). In addition, Pt clusters of d = 1.0 ± 0.2 nm were identified on Al_2O_3 (Figure 2d,e). For a comparison, on non-diluted Pt/Al_2O_3 used in 400 °C rWGS, we found larger Pt clusters of d = 1.4 ± 0.2 nm and no single Pt atoms (Figure 2f). The comparison of the two samples suggests that some Pt migrate onto TiO_2 during the rWGS, increasing Pt dispersion, and thus the reaction rate. The observation is surprising as the intersupport-particle migration of noble metals has been rarely recognized under reducing atmospheres or at <600 °C.[15] We note that noble metals are known to be more active for the rWGS on TiO_2 than on Al_2O_3 despite following the same mechanism, as more metal−support interfacial (MSI) sites can be formed on reducible supports.[30] This likely also contributes to the higher pre-exponential factor and thus the higher rWGS rate, along with the increased Pt dispersion.

https://doi.org/10.1021/acscatal.1c03133
ACS Catal. XXXX, XXX, XXX−XXX

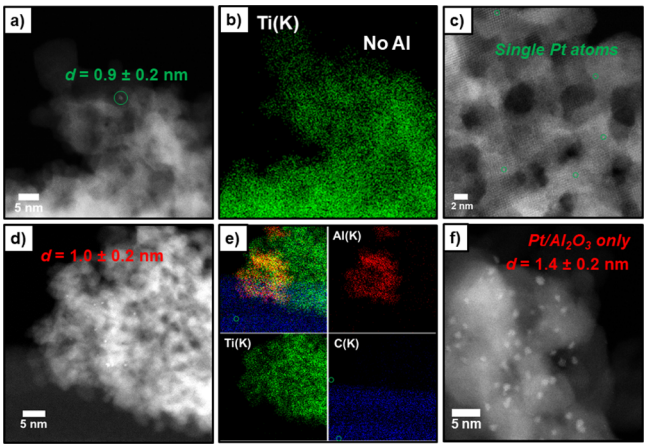

Figure 2. STEM and EDX images after 400 °C rWGS for 1 h (reaction conditions identical with Figure 1). All images were obtained on Pt/Al_2O_3 + A-TiO_2 = 1:10, except for panel (f), which was obtained on Pt/Al_2O_3 only. Three categories of STEM images were identified on Pt/Al_2O_3 + A-TiO_2. Panel (a) shows an example of the first category, in which Pt clusters (in the green circle) were found in an area identified by EDX in panel (b) as TiO_2. The average diameter of similar clusters is 0.9 ± 0.2 nm. Panel (c) shows an example of the second category, in which features resembling single Pt atoms were found (in green circles). This area is likely TiO_2 based on the lattice diffraction. Panel (d) shows an example of the third category, in which Pt clusters were found in an area identified by EDX in panel (e) as overlapping TiO_2 and Al_2O_3. The average diameter of similar clusters is 1.0 ± 0.2 nm. Although panel (e) shows that the area has both TiO_2 and Al_2O_3, Pt are exclusively located in regions where Al is present, suggesting that Pt are highly likely on Al_2O_3. Panel (f) shows a representative image of Pt/Al_2O_3 only after the same reaction, in which dense Pt clusters of average diameter of 1.4 ± 0.2 nm were found.

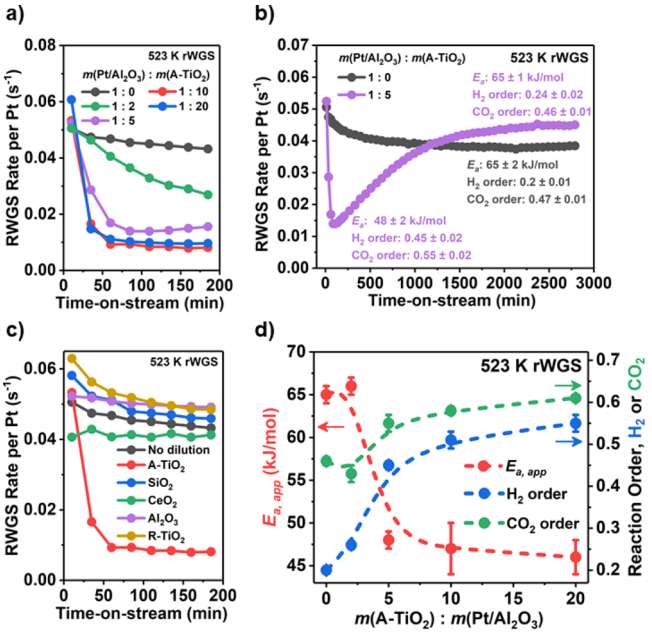

Figure 3. Kinetic data of the rWGS reaction over diluted 2% Pt/Al_2O_3 at 250 °C. Panel (a) shows variations in the per-Pt rWGS rate with TOS, with a varying amount of A-TiO_2 as the dilutant. Panel (b) shows the extended version of (a) on selected samples to 2 days TOS. Panel (c) shows variations in the per-Pt rWGS rate with time, with different oxides of 10 times mass of Pt/Al_2O_3 as the dilutant. Because R-TiO_2 only has less than 1/10 of the surface area of A-TiO_2 (Table S1), the R-TiO_2 measurement was repeated with a higher dilution factor (170) that equates the surface area of A-TiO_2 per g Pt/Al_2O_3 and shows similar results. Panel (d) summarizes kinetic parameters (red: $E_{a,app}$, blue: H_2 order, green: CO_2 order) at the lowest point of each curve in panel (a) (fitting plots shown in Figure S7). Reaction conditions are identical with Figure 1.

We tested the generalizability of the Al_2O_3-to-dilutant Pt migration. Figure 1c shows that dilution with all the tested oxides except for SiO_2, that is, CeO_2, Al_2O_3, and rutile TiO_2 ("R-TiO_2", see Table S1 for the surface area), enhances the activity of Pt/Al_2O_3, both at 400 °C (blue) and at 250 °C after the 400 °C reaction (red), indicating that Pt can migrate onto not only A-TiO_2. On the other hand, Figure 1d suggests that low-loading Pt/Al_2O_3 (0.05 to 0.25 wt % Pt, synthesized by strong electrostatic adsorption) catalysts, on which a large fraction of Pt are sub-nanometer Pt clusters and single atoms (Figure S4) and also clearly exhibit higher activity with TiO_2 dilution, suggesting that highly dispersed Pt can migrate onto TiO_2 as well. We note that the rate enhancement is not only observed after 400 °C rWGS but also after the 400 °C H_2 treatment, to a lesser extent (Table S2), implying that Pt migrate in reduced forms, and their mobility is enhanced by CO produced from the rWGS. Overall, our data show that during the rWGS at 400 °C, Pt migrate from Al_2O_3 to oxide dilutants, improving the dispersion and catalytic activity without changing the reaction mechanism.

2.2. rWGS at 250 °C: Acetate Transfer Reducing Activity and Altering Reaction Mechanism. *2.2.1. Contamination Transfer from TiO_2 Deactivating Pt/Al_2O_3.* Interestingly, kinetic data collected at 250 °C exhibited a completely different behavior from those obtained at 400 °C. Figure 3a shows that the per-Pt rWGS rate on all Pt/Al_2O_3 + A-TiO_2 samples decreases quickly with TOS to <20% of the initial rate after 2 h with dilution factor ≥ 10. Exposing the deactivated samples to room-temperature air does not alter the activity (Figure S5). Nonetheless, further performing the rWGS on Pt/Al_2O_3 + A-TiO_2 at 250 °C leads to a slow but complete activity recovery, as the rate is stabilized after 2 days TOS, at a level close to the rate on Pt/Al_2O_3 only (Figure 3b). Unlike the Pt migration at 400 °C, the dilution-induced deactivation at 250 °C is mostly unique to A-TiO_2 (Figure 3c): CeO_2 and Al_2O_3 exhibit negligible impacts on the rWGS rate, while SiO_2 and R-TiO_2 have much less severe effects than A-TiO_2. Meanwhile, A-TiO_2 also deactivates other Pt catalysts, including 0.05−0.25 wt % Pt/Al_2O_3 (less severe with a higher Pt dispersion, Figure S6a), as well as 2 wt % Pt/CeO_2 and Pt/SiO_2 (Figure S6b). The unique effect of A-TiO_2 in deactivating Pt catalysts at 250 °C, particularly the contrast with CeO_2 and R-TiO_2, indicates that the deactivation is associated with the surface properties of A-TiO_2 instead of its reducibility.

Figure 3d shows that the kinetic parameters on Pt/Al_2O_3 + A-TiO_2 at 250 °C, measured at the lowest point of the curves in Figure 3a, are drastically different from those on Pt/Al_2O_3 only: as the dilution factor increases from 0 to 20, $E_{a,app}$ drops from ∼66 to ∼47 kJ/mol, H_2 and CO_2 orders increase from ∼0.2 to ∼0.55, and from ∼0.45 to ∼0.61, respectively. Juxtaposed with the identical kinetic parameters on these samples at 250 °C after 400 °C rWGS (Figure 1b), the clear trends in Figure 3d suggest that the TiO_2-induced deactivation at 250 °C changes the reaction mechanism, rather than merely the number and location of active sites. In addition, Figure 3b shows that the recovery of rate on Pt/Al_2O_3 + TiO_2 after 2 days TOS is accompanied by the recovery of all kinetic

https://doi.org/10.1021/acscatal.1c03133
ACS Catal. XXXX, XXX, XXX−XXX

parameters to values close to those found on Pt/Al_2O_3 only. We note that Pt sintering does not likely contribute to the deactivation, as (1) it is difficult to rationalize more severe sintering with a higher dilution factor and (2) sintering cannot explain the rate recovery after long TOS.

The dilutant-to-catalyst contamination transfer was invoked in the literature to explain the reduced rate with dilution.[16,28] To test the theory, we examined Pt/Al_2O_3 + A-TiO_2 with various reactor configurations (Figure 4a), with results

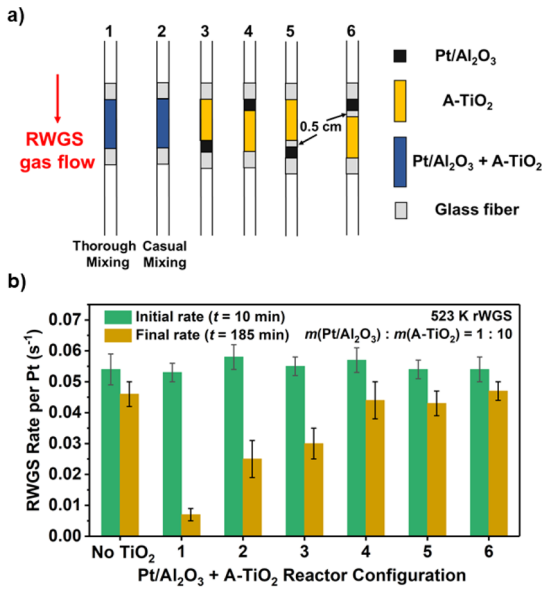

Figure 4. rWGS testing results at 250 °C on 2% Pt/Al_2O_3 and A-TiO_2 10 times its mass, with various reactor configurations. Panel (a) shows the schematic drawing of each configuration. In configuration 2, the two components were mixed in a weighing paper with a spatula instead of in a mortar with a pestle (configuration 1). Panel (b) summarizes the rWGS activity at 250 °C, with green and yellow bars representing the initial (t = 10 min) and final (t = 185 min) rates, respectively (rate *vs* TOS shown in Figure S8). Error bars represent standard deviations from 2 or 3 repetitions of each experiment, and data in Figure S8 are the average of the runs. Reaction conditions are identical with in Figure 1.

summarized in Figure 4b. Configurations 3 and 4 show that when Pt/Al_2O_3 and TiO_2 are loaded into one bed sequentially without separation or intentional mixing, the deactivation is more severe when TiO_2 is placed at the upstream of Pt/Al_2O_3 than downstream, consistent with the contamination transfer. Besides, the theory also explains the slow activity recovery after the deactivation in Figure 3b: the contaminant is transferred onto Pt/Al_2O_3 first and then slowly desorbs. Figure 4 also indicates that the contamination transfer has a short range, as the deactivation is (1) significantly less severe when the two components are "casually mixed" (configuration 2, mixed with a spatula) than when "thoroughly mixed" (configuration 1, ground with a pestle) and (2) subtle when the two components are separated by 0.5 cm glass fibers (configuration 5 and 6 compared to "No TiO_2"). Therefore, the contaminant is not likely transferred as stable gas-phase molecules. Instead, it probably moves either via diffusion between oxide particles in close contact, or through radicals with a short lifetime.

2.2.2. Unveiling the Identity of the "Carbon Contaminant" on TiO_2: Acetic Acid (Acetate). The dilutant-to-catalyst contamination transfer was reported 40 years ago but rarely investigated since,[16,28] so the identity of the "carbon contaminant", how it migrates between oxides or its impact on catalysis have yet to be explained. We will address these aspects here. To begin with, TiO_2 surfaces are known for the strong affinity toward carboxylic acids.[31−33] As a result, formic/acetic acids (AAs) in air, despite only present at a ppm level,[34] lead to formate/acetate layers on TiO_2 surfaces.[35] This is supported by the infrared (IR) spectrum of A-TiO_2 under vacuum, which shows a triplet of bands in the ν(CH) region at 2963, 2928, and 2854 cm^{-1} (Figure S9a), consistent with formic/AAs adsorbed on oxides.[36−42] Bands between 1200 and 1600 cm^{-1} could also arise from formate/acetate (Figure S9b).[37,39,41−44] As a rWGS intermediate, formate reacts with H_2 quickly[11,12,45,46] and thus should not poison Pt/Al_2O_3. We confirmed this by pre-adsorbing formic acid (FA) onto Pt/Al_2O_3 (Scheme S1, sample referred to as "Pt/Al_2O_3-FA") and then tested it for 250 °C rWGS. Figure 5a shows that after 4 h of air exposure, the rWGS rates on Pt/Al_2O_3-FA and clean Pt/Al_2O_3 are very similar. In contrast, the deactivation effect of the contaminant from TiO_2 persists after 2 days of air exposure (Figure S5). Furthermore, Pt/Al_2O_3-FA does not show an increasing rWGS rate with TOS (Figures 5a and S10a), a fingerprint of TiO_2-contaminated Pt/Al_2O_3 (Figure 3b). The discrepancy between results on Pt/Al_2O_3-FA and TiO_2-contaminated Pt/Al_2O_3 exonerate FA as the poisoning "carbon contaminant" on TiO_2.

In contrast, Pt/Al_2O_3 pre-adsorbed with AA ("Pt/Al_2O_3-AA") exhibits behaviors that highly resemble TiO_2-contaminated Pt/Al_2O_3. The initial rWGS rate on Pt/Al_2O_3-AA (Figure 5b, red, no rate change after 3 days air exposure in Figure S10b) is significantly lower than that on clean Pt/Al_2O_3 (~0.05 s^{-1} per Pt) and close to the lowest rate on Pt/Al_2O_3 + A-TiO_2 = 1:5 (blue), indicating that adsorbed AA causes similar deactivation to Pt/Al_2O_3 with the contaminant originating from TiO_2. Also, on both Pt/Al_2O_3-AA and deactivated Pt/Al_2O_3 + A-TiO_2, the rate increases slowly with TOS, indicating that both AA and the contaminant from TiO_2 gradually desorb during 250 °C rWGS. Furthermore, both AA and the contaminant from TiO_2 are partially removed from Pt/Al_2O_3 by 150 °C air, shown by the partial re-activation of both Pt/Al_2O_3-AA and Pt/Al_2O_3 + A-TiO_2 after such treatment (Figure 5c). The strikingly similar effects of pre-adsorbed AA and the contaminant from TiO_2 on Pt/Al_2O_3 strongly imply that AA (acetate) is the poisoning "carbon contaminant". Furthermore, we tested an A-TiO_2 with pre-adsorbed AA ("A-TiO_2-AA") before mixing with Pt/Al_2O_3, and A-TiO_2 synthesized using AA for phase control and not calcined ("AA-TiO_2").[47] Figure 5c shows that the dilution with both A-TiO_2 with higher acetate coverage leads to faster and more severe deactivation than with normal A-TiO_2, proving that acetate adsorbed on TiO_2 can be transferred to Pt/Al_2O_3 during the 250 °C rWGS, further indicating acidic acid (acetate) as the poisoning "carbon contaminant" on TiO_2.

2.2.3. TiO_2 Dilution Blocking the Formate rWGS Pathway. As Figure 3b suggests A-TiO_2 dilution changes the rWGS mechanism on Pt/Al_2O_3 at 250 °C. Therefore, we examined the mechanistic consequences of TiO_2 dilution by *operando* diffuse reflectance IR spectroscopy (DRIFTS). Figure 6a shows the evolution of DRIFT spectra on Pt/Al_2O_3 only during 250 °C rWGS (background collected at 250 °C in He). Upon the introduction of the rWGS stream, two Al_2O_3-bound species form quickly: bicarbonate (green labels), shown by bands at 1230 [γ(COH)], 1435 [$\nu(OCO)_{sym}$, B1 type], 1469

https://doi.org/10.1021/acscatal.1c03133
ACS Catal. XXXX, XXX, XXX−XXX

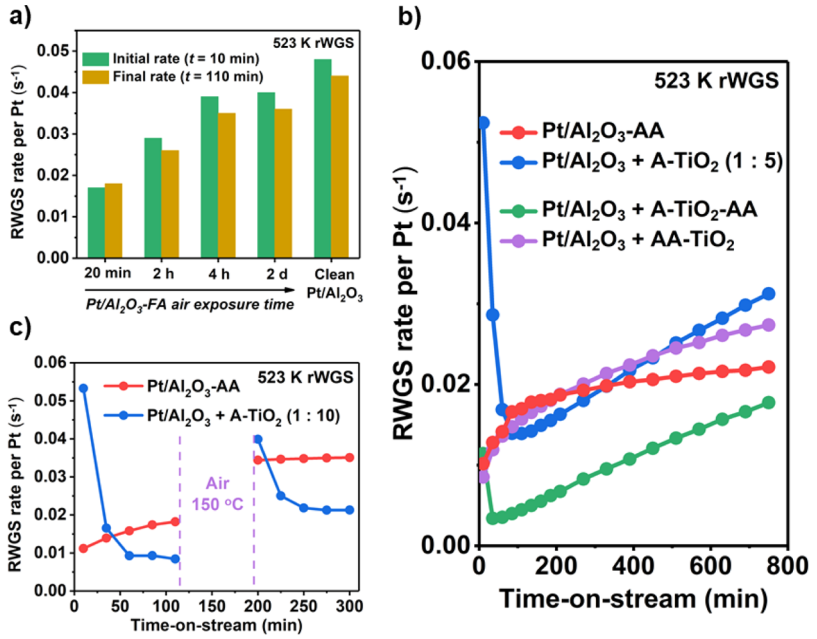

Figure 5. rWGS testing results at 250 °C on 2% Pt/Al_2O_3 intentionally contaminated by FA or AA. Panel (a) shows the rWGS rate on Pt/Al_2O_3 after overnight FA adsorption followed by room-temperature air exposure for various time. Green and yellow bars represent the initial (t = 10 min) and final (t = 110 min) rates, respectively (rate *vs* TOS shown in Figure S10a). Panel (b) shows variations in the rWGS rate with TOS on Pt/Al_2O_3 after overnight AA adsorption (red), Pt/Al_2O_3 diluted with commercial A-TiO_2 (blue, 1:5), Pt/Al_2O_3 diluted with commercial A-TiO_2 that went through overnight AA adsorption (green), and Pt/Al_2O_3 diluted with an A-TiO_2 synthesized with a AA-assisted sol−gel method without calcination (purple). For the three diluted samples, the TiO_2 surface area per g Pt/Al_2O_3 is identical. Panel (c) shows variations in the rWGS rate with TOS on Pt/Al_2O_3 after overnight AA adsorption (red) and Pt/Al_2O_3 diluted with the commercial A-TiO_2 (blue, 1:10), after an air treatment at 150 °C that re-activates the catalysts.

[ν(OCO)$_{sym}$, B2 type], 1648 [ν(OCO)$_{asym}$], and 3610 cm^{-1} [ν(COH), shown in Figure S11a], and carbonate (yellow labels), shown by bands at 1770 [ν(OCO)$_{asym}$] and 1511 cm^{-1} [ν(OCO)$_{sym}$].[48,49] As the reaction proceeds, the intensity of these bands decreases, while bands from Al_2O_3-bound formates (*HCOO, red labels for bridging, blue labels for monodentate, and purple labels for shared bands) at 1359 [ν(OCO)$_{sym\text{-}mono}$], 1375 [ν(OCO)$_{sym\text{-}br}$], 1392 [δ(CH)], 1591 [ν(OCO)$_{asym\text{-}br}$], 1625 [ν(OCO)$_{asym\text{-}mono}$], 2763, 2904, and 2993 cm^{-1} [ν(CH), shown in Figure S11a] rise gradually.[11,38,43,44] Therefore, CO_2 adsorption leads to bicarbonate and carbonate initially, which are hydrogenated into formates that accumulate under reaction conditions.[11,12,45,46] Meanwhile, a broad, asymmetric band centered at 2032 cm^{-1} accumulates with time, which is from carbonyl (*CO) bound to various Pt sites.

After 2 h rWGS, CO_2 was turned off, and the evolution of DRIFT spectra was monitored and shown in Figures 6b and S11b. Without CO_2, bands from bicarbonate, carbonate, and monodentate formate disappear quickly. Based on previous studies, bicarbonate and carbonate disappear due to the desorption of weakly adsorbed CO_2, while monodentate formate reacts with H_2 yielding CO and H_2O, known as the "formate pathway" of the rWGS.[12,45,46,48,49] In contrast, bands from bridging formate decrease slowly, suggesting that it reacts with H_2 at a much lower rate. Such observations indicate that at 250 °C, monodentate formate is a highly reactive rWGS intermediate, while bridging formate is more stable and thus contributes less, aligning well with previous work on Pd/Al_2O_3.[11] Meanwhile, the same work also suggested the existence of a second rWGS pathway—the "carboxyl (*COOH) pathway" at the MSI, with IR-elusive carboxyl intermediate.[11] We note that the carbonyl band barely changes without CO_2, indicating that it is from CO that are strongly bound to Pt and thus do not desorb. In summary, DRIFTS suggest that on Pt/Al_2O_3 without TiO_2, the formate pathway has significant contribution to the rWGS, with monodentate formate as the most reactive intermediate. Bridging formate accumulates on Al_2O_3 but reacts with H_2 slowly.

Figures 6c and S11c show DRIFT spectra on Pt/Al_2O_3 + A-TiO_2 during 250 °C rWGS. The carbonyl band at 2032 cm^{-1} accumulates with time, indicating that *CO is formed. However, formate bands are not present, that is, formates cannot form on Al_2O_3 with TiO_2 dilution. The wide bands between 1300 and 1550 cm^{-1} in Figure 6c are assigned to TiO_2-bound *H_xCO_y species, as they are also present on TiO_2 only under identical conditions (Figures 6d and S11d). Without CO_2, the intensity of these bands drops similarly with and without Pt/Al_2O_3 (Figure S11e,f). Because TiO_2 only has negligible rWGS activity (Figure S1), the observations suggest that the TiO_2-bound species still do not contribute to the rWGS when mixed with Pt/Al_2O_3. Besides, Figure 6e shows that after 250 °C rWGS, IR bands from CO adsorption on Pt/Al_2O_3 and Pt/Al_2O_3 + A-TiO_2 are of similar shape. Also, in Figures 6a,c, the 2032 cm^{-1} Pt−CO band during the rWGS on the two samples is also of identical shape. Therefore, TiO_2 does not alter the distribution of Pt sites available to CO, eliminating the possibility that the deactivation is due to the selective poisoning of Pt sites or significant Pt sintering.

Figure 6 reveals that TiO_2 deactivates Pt/Al_2O_3 by blocking the formate formation on Al_2O_3. This is logical as acetate should occupy the same sites as formates but does not react with H_2 quickly.[50] In addition, X-ray photoemission spectra (XPS) in the C 1s region (Figure 7) show that on Pt/Al_2O_3 only, after 250 °C rWGS, the area of the ~289 eV component

https://doi.org/10.1021/acscatal.1c03133
ACS Catal. XXXX, XXX, XXX−XXX

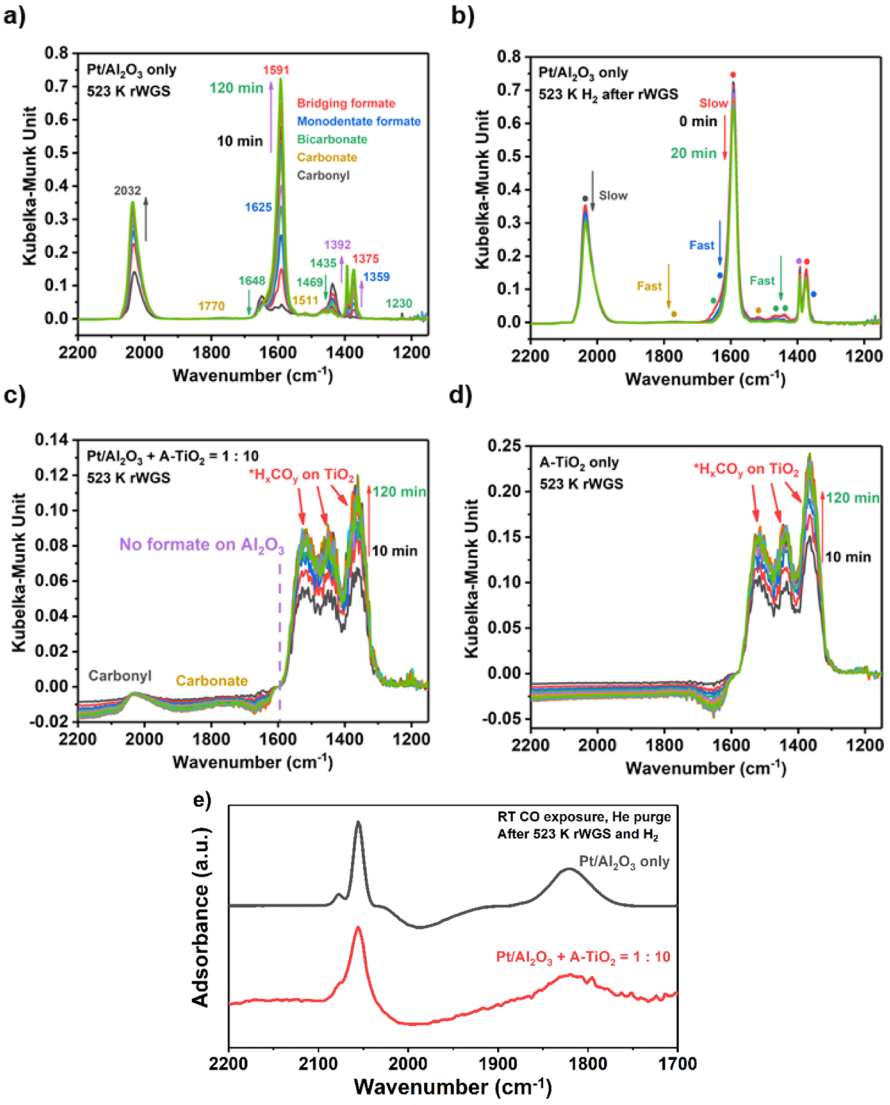

Figure 6. *Operando* DRIFTS results on Pt/Al_2O_3 only and Pt/Al_2O_3 + A-TiO_2 = 1:10 at 250 °C. Panel (a) shows DRIFT spectra on Pt/Al_2O_3 only during the rWGS for 2 h, with each spectrum separated by 10 min. Panel (b) shows DRIFT spectra under 250 °C H_2 after (a), with each spectrum separated by 2 min. Panels (c,d) show the same spectra with (a), on Pt/Al_2O_3 + A-TiO_2 = 1:10 and A-TiO_2 only, respectively. Panel (e) shows the CO adsorption (after He purge, normalized to similar intensity) DRIFT spectra at room temperature after the reaction on both samples. Supporting Information can be found in Figure S11. Experiment conditions: 250 °C, CO_2/H_2/He = 1:4:15, total flow rate = 32 sccm vented to ambient pressure.

from O−C═O types of carbon significantly increases (Figure 7a), which is attributed to formate accumulation shown in Figure 6a. In contrast, on Pt/Al_2O_3 + A-TiO_2, the area of this component does not increase after the rWGS (Figure 7b), consistent with the lack of formate formation shown in Figure 6c. Despite the blocking of the formate pathway, Pt/Al_2O_3 + A-TiO_2 still exhibits rWGS activity (Figure 3a), and DRIFTS show *CO formation (Figure 6c), supporting the presence of a second rWGS pathway, that is, the carboxyl pathway. Although this pathway is not definitively observed in Figure 6, as the intermediate is IR elusive, it has been proven previously.[11] This explains the kinetic parameters shown in Figure 3d: at 250 °C on Pt/Al_2O_3, the rWGS mainly follows the formate pathway ($E_{a,app}$ ~ 66 kJ/mol, H_2 order ~ 0.2, CO_2 order ~ 0.45), as shown on Pd/Al_2O_3.[11,12,45,46] With formate formation blocked by TiO_2 dilution, the rWGS can only follow the carboxyl pathway and thus, the kinetic parameters change ($E_{a,app}$ ~ 47 kJ/mol, H_2 order ~ 0.55, CO_2 order ~ 0.61). The desorption of acetate after long TOS restores the formate pathway, so when the rate is recovered, the kinetic parameters also recover (Figure 3b, after 2 days TOS).

2.2.4. Stability and Removal of Acetate Adsorbed on TiO_2. The acetate transfer prevents us from investigating other catalyst−dilutant communication effects. Therefore, it is necessary to understand the stability of acetate adsorbed on TiO_2. Figure 8a shows that after a 250 °C, 3 h CO_2 + He treatment (black), Pt/Al_2O_3 + A-TiO_2 exhibits a similar rate and deactivation with the fresh sample (red). In contrast, a 250 °C, 3 h H_2 + He treatment induces significant deactivation (blue). Therefore, the acetate transfer is mainly facilitated by H_2 in the rWGS stream. Besides, Figure 8b shows that treating Pt/Al_2O_3 + A-TiO_2 with H_2 at 300 °C for 12 h leads to a steady rWGS rate (green) at a similar level with Pt/Al_2O_3 only (~0.05 s^{-1} per Pt), indicating complete acetate removal, further exhibiting its instability under H_2. In contrast, after a 300 °C, 12 h air treatment, Pt/Al_2O_3 + A-TiO_2 still exhibits

https://doi.org/10.1021/acscatal.1c03133
ACS Catal. XXXX, XXX, XXX−XXX

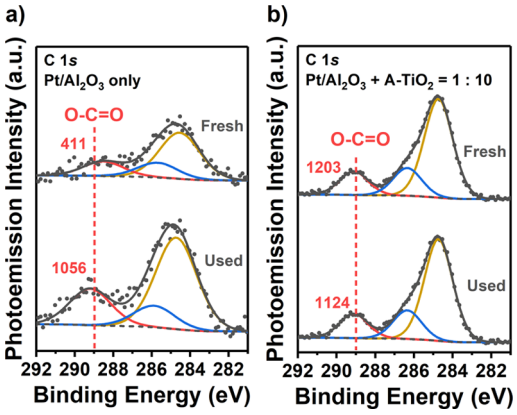

Figure 7. XP spectra in the C 1s region of (a) Pt/Al_2O_3 only and (b) Pt/Al_2O_3 + A-TiO_2 = 1:10. In both graphs, the top spectrum was collected on the fresh sample, and then the sample was treated at 250 °C by the rWGS mixture (CO_2 + H_2 + He = 1:4:15) in an attached side chamber for 3 h. After cooling down to room temperature under He, the sample was transferred back into the XPS chamber without air exposure, and the bottom spectrum was collected on the used sample. The area of the ~289 eV from O−C═O type of C was labeled as red.

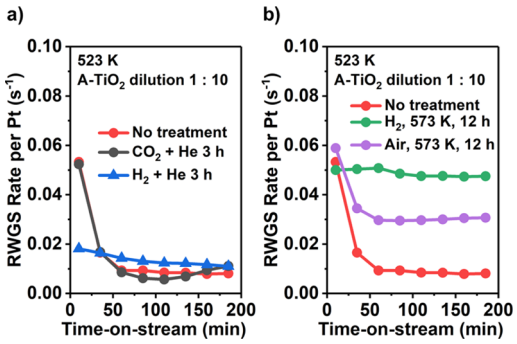

Figure 8. Variations of the rWGS rate with TOS at 250 °C on Pt/Al_2O_3 + A-TiO_2 = 1: 10 after different pretreatments. Panel (a) shows results with the pretreatment of 5% CO_2 in He for 3 h (black), and 20% H_2 in He for 3 h (blue) at 250 °C, to compare with results with no pretreatment (red). Panel (b) shows results with a pretreatment of 20% H_2 in He for 12 h (purple) and air for 12 h (green) at 300 °C, to compare with results with no pretreatment (red). Reaction conditions are identical with Figure 1. H_2 or CO_2 concentration in the pretreatment stream is identical with the concentration in the rWGS stream.

deactivation to a lesser degree than the fresh sample (purple compared to red), suggesting only partial acetate removal, that is, acetate adsorbed on TiO_2 is less stable under H_2 than air. As demonstrated above, heating Pt/Al_2O_3 + A-TiO_2 to 400 °C results in Pt migration. Therefore, we cleaned TiO_2 by itself at 400 °C before mixing it with Pt/Al_2O_3 with minimal air exposure. The results in Figure S12b again show that TiO_2 cleaned by H_2 deactivates Pt/Al_2O_3 less, that is, has a lower acetate coverage, than TiO_2 cleaned by air, further verifying that H_2 treatment is the more effective strategy for acetate removal.

3. DISCUSSION

3.1. Multiple Pathways of the Catalyst−Dilutant Communication. Three types of species were proposed to migrate between the catalyst and the dilutant: (1) "carbon contaminant",[16,28] (2) metal sites,[15] and (3) activated H.[17−22] The contrast between our results at 400 and 250 °C highlights the complicacy of the catalyst−dilutant communication, showing that multiple processes could occur in one system under different conditions. Therefore, one should be cautious about potential pitfalls when assigning catalytic effects to or studying one of them independently. With appropriate analysis of our results, intriguing insights were obtained regarding each of the processes, which will be discussed separately below.

The selective adsorption of the ppm level carboxylic acids in air by TiO_2 was recognized.[35] The deactivation at 250 °C presented here shows that the formate/acetate layers could affect catalysis for the first time and in these cases, their removal (most facile under H_2) is necessary for optimal catalyst performance. According to Figures 6, 7, and S11, acetate deactivates Pt/Al_2O_3 for the rWGS by blocking formate binding sites on Al_2O_3 but not likely by poisoning or sintering Pt. Therefore, it should affect reactions involving formate or intermediates bound on similar support sites but may not impact reactions that occur completely on metal sites. The acetate transfer was not captured by DRIFTS (Figure 6c), likely because of similar IR signatures from A-TiO_2- and Al_2O_3-bound acetates. Also, to block the formate formation, acetate probably only needs to occupy sites near Pt, which are not abundant, and thus the fraction of acetate that moved onto Al_2O_3 is likely not large. In addition, the fact that R-TiO_2 induces a less severe deactivation than A-TiO_2 (Figure 3b) is intriguing, as carboxylic acids should dissociatively adsorb on both phases of TiO_2.[32,39,51,52] This might be due to the stronger adsorption of acetate on R-TiO_2 that limits its transfer to Pt/Al_2O_3.[39,51]

The Pt migration from Al_2O_3 to A-TiO_2 during 400 °C rWGS shown in this work echoes with the Pd migration among P25 TiO_2 particles under similar conditions.[15] Nonetheless, Pd carbonyl has high mobility on oxide surfaces,[53] while Pt carbonyl does not.[54] Also, conventional wisdom is that Pt moves between oxides under O_2 at ≥600 °C as volatile PtO_x.[55−57] Therefore, the inter-oxide Pt migration under reducing conditions at 400 °C was unexpected, emphasizing that the dynamics of metal atoms during catalysis is underappreciated. On support surfaces, metal adatoms are always at equilibrium with clusters, acting as the mobile intermediate for nuclearity changes.[58−61] Due to the low vapor pressure of reduced Pt, Pt adatoms should not migrate through the gas phase. Instead, they likely diffuse between oxides in close contact, which are facilitated by forming more mobile carbonyls.[53,62] Nonetheless, the barrier of inter-oxide diffusion is still high enough so that the process does not occur below 250 °C (Figure 3). This mechanism is supported by the observation that when A-TiO_2 is placed in a separated bed downstream of Pt/Al_2O_3, no rate enhancement was observed at 400 °C. Also, it predicts that Pt would migrate regardless of the identity of the dilutant. Nevertheless, the binding strength of the dilutant to Pt should affect the equilibrated Pt species. With SiO_2 dilution, which binds Pt weakly, less Pt migrate and Pt could sinter severely, thus leading to the lack of rate enhancement in Figure 1c.

Debates over whether inter-oxide H spillover occurs remain unsettled.[10,16−22,26] A recent study suggested that activated H on Ni/R-TiO_2 are transferred onto Ni-free A-TiO_2 as gas-phase radicals, activating A-TiO_2 for CO_2 methanation.[19] Our results emphasize that related discussions require acetate-free materials, for example, the sample after 300 °C, 12 h H_2 cleaning in this work, and a low temperature to avoid metal

https://doi.org/10.1021/acscatal.1c03133
ACS Catal. XXXX, XXX, XXX−XXX

migration, for example 250 °C. In Figures 3b and 8b, clean Pt/Al_2O_3 + A-TiO_2 exhibits similar activity with Pt/Al_2O_3 only. Besides, DRIFTS (Figures 6c,d and S11c,d) suggest that the property of TiO_2-bound H_xCO_y species is not altered by mixing with Pt/Al_2O_3. Therefore, there is no evidence that A-TiO_2 accepts activated H from Pt/Al_2O_3 and participates in the rWGS. Nevertheless, clean 2% Pt/CeO_2 + A-TiO_2 does show a higher rWGS rate than Pt/CeO_2 only (Figure S13), a possible sign of A-TiO_2 being activated by H transfer. The contrast suggests that if H are transferred onto and activate A-TiO_2, they are likely shuttled by the support, which is facilitated by the reducibility of CeO_2, instead of as gas-phase radicals.[19] This is supported by the lack of rate enhancement when A-TiO_2 is placed in a separated bed downstream of Pt/CeO_2 (Figure S13). It can also explain the observation that increasing the dilution factor from 10 to 50 does not change the rate on Pt/CeO_2 + A-TiO_2 (Figure S13), as only A-TiO_2 in close contact with CeO_2 can accept H shuttled by CeO_2. Overall, our results imply that inter-oxide H spillover is only likely from reducible CeO_2 to A-TiO_2, consistent with thermodynamic predictions.[10,26]

3.2. TiO_2 Dilution Validating the Dual-Pathway rWGS Mechanism. As shown by DRIFTS (Figures 6 and S11), the formate rWGS pathway is blocked by acetate transfer, which offers an opportunity to deconvolute it from the carboxyl pathway and measure the kinetic parameters of each separately (Figure 3d).[11] It has been shown that the carboxyl pathway occurs at the MSI sites, while the formate pathway requires continuous metal sites.[11,12,45,46] The conclusion predicts that under identical conditions, the carboxyl pathway contributes more on smaller metal clusters, as the ratio between the MSI sites and continuous metal sites is higher. This is supported by the observation that the blocking of the formate pathway affects smaller Pt clusters less (Figure S6a). Following this reasoning, we measured the reaction orders on a series of low-loading Pt/Al_2O_3 (without dilution). Figure 9 shows that as

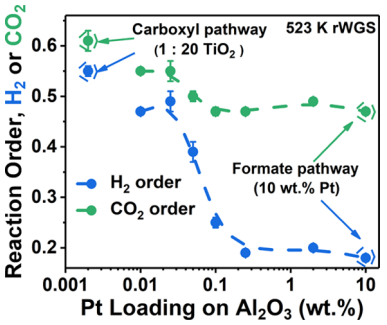

Figure 9. Variations in the dependence of the rWGS rate on the partial pressure of H_2 (blue) and CO_2 (green) at 250 °C with Pt loading on Pt/Al_2O_3. Fitting plots can be found in Figure S14. The data on Pt/Al_2O_3 + A-TiO_2 = 1:20 in Figure 3d, on which the formate pathway is blocked, were used for the "carboxyl pathway" data.

the Pt loading decreases, that is, Pt clusters become smaller, both H_2 and CO_2 orders move from those of the formate pathway, to those of the carboxyl pathway, consistent with the prediction. In addition, we have suggested that because the H_2 dissociation in the carboxyl pathway has a high barrier, it becomes important only at a high temperature (T > 300 °C),[11] consistent with that at 250 °C, blocking the formate pathway leads to >80% turnover rate loss (Figure 3a), and the higher H_2 order for the carboxyl pathway (0.55) than the formate pathway (0.18). Overall, our results lead to new evidence that strengthens the validity of and provides more details on the dual-pathway rWGS mechanism.

4. CONCLUSIONS

In this work, we demonstrated the temperature-dependent communication between the 2% Pt/Al_2O_3 catalyst and A-TiO_2 dilutant and its impacts on the rWGS reaction. During 400 °C rWGS, Pt migrates from Al_2O_3 to A-TiO_2 or other oxide dilutants except for SiO_2, enhancing the activity but not altering the mechanism. During 250 °C rWGS, the "carbon contaminant" moves from A-TiO_2 to Al_2O_3, deactivating Pt/Al_2O_3. Spectroscopic and kinetic data suggested that the "carbon contaminant" is acetate adsorbed from air, the inter-oxide transfer of which requires close contact and the assistance of H_2. The acetate blocks the formation sites for formate on Al_2O_3, the intermediate of the dominant rWGS pathway at 250 °C. The kinetic data on TiO_2-diluted Pt/Al_2O_3 align well with the proposed rWGS mechanism that involves both the formate pathway (dominating at low temperatures) and the carboxyl pathway at the metal−support interface (dominating at high temperatures). After acetate removal, Pt/Al_2O_3-to-TiO_2 H spillover was not definitively observed but CeO_2 likely shuttles activated H from Pt to A-TiO_2 with its reducibility. This work reveals how a supposedly "inert" oxide dilutant could affect catalysis at different temperatures, helping understand the impactful but rarely explored catalyst−dilutant communication, reconcile contradictory results and debates in the literature and clear potential pitfalls in related investigations. In addition, it provides unique new evidence that further elucidates the rWGS mechanism.

■ ASSOCIATED CONTENT

Supporting Information

Experimental methods and detailed kinetic and spectroscopy data (PDF) The Supporting Information is available free of charge at https://pubs.acs.org/doi/10.1021/acscatal.1c03133.

(PDF)

■ AUTHOR INFORMATION

Corresponding Author

János Szanyi − *Institute for Integrated Catalysis, Pacific Northwest National Laboratory, Richland, Washington 99352, United States;* orcid.org/0000-0002-8442-5465; Email: janos.szanyi@pnnl.gov

Authors

Linxiao Chen − *Institute for Integrated Catalysis, Pacific Northwest National Laboratory, Richland, Washington 99352, United States*

Libor Kovarik − *Institute for Integrated Catalysis, Pacific Northwest National Laboratory, Richland, Washington 99352, United States*

Complete contact information is available at: https://pubs.acs.org/10.1021/acscatal.1c03133

Notes

The authors declare no competing financial interest.

■ ACKNOWLEDGMENTS

This work was supported by the U.S. Department of Energy (DOE), Office of Science, Office of Basic Energy Sciences,

Division of Chemical Sciences, Geosciences, and Biosciences and performed at the Environmental Molecular Sciences Laboratory in (EMSL), which is a DOE Office of Science User Facility located at Pacific Northwest National Laboratory (PNNL). PNNL is a multiprogram national laboratory operated for DOE by Battelle. We acknowledge Mark H. Engelhard, Dr. Mark E. Bowden, Dr. Nicholas C. Nelson, and Shari Xiaohong Li at PNNL for assisting XPS, XRD, DRIFTS, and BET measurements.

REFERENCES

(1) van Deelen, T. W.; Hernández Mejía, C.; de Jong, K. P. Control of metal-support interactions in heterogeneous catalysts to enhance activity and selectivity. *Nat. Catal.* **2019**, *2*, 955−970.

(2) Tauster, S. J.; Fung, S. C.; Baker, R. T. K.; Horsley, J. A. Strong Interactions in Supported-Metal Catalysts. *Science* **1981**, *211*, 1121−1125.

(3) Liu, P.; Zhu, X.; Yang, S.; Li, T.; Hensen, E. J. M. On the metal−support synergy for selective gas-phase ethanol oxidation over $MgCuCr_2O_4$ supported metal nanoparticle catalysts. *J. Catal.* **2015**, *331*, 138−146.

(4) Primo, A.; Concepción, P.; Corma, A. Synergy between the metal nanoparticles and the support for the hydrogenation of functionalized carboxylic acids to diols on Ru/TiO2. *Chem. Commun.* **2011**, *47*, 3613−3615.

(5) Hu, P.; Huang, Z.; Amghouz, Z.; Makkee, M.; Xu, F.; Kapteijn, F.; Dikhtiarenko, A.; Chen, Y.; Gu, X.; Tang, X. Electronic Metal−Support Interactions in Single-Atom Catalysts. *Angew. Chem., Int. Ed.* **2014**, *53*, 3418−3421.

(6) Campbell, C. T. Electronic perturbations. *Nat. Chem.* **2012**, *4*, 597−598.

(7) He, H.; Chen, J.; Zhang, D.; Li, F.; Chen, X.; Chen, Y.; Bian, L.; Wang, Q.; Duan, P.; Wen, Z.; Lv, X. Modulating the Electrocatalytic Performance of Palladium with the Electronic Metal−Support Interaction: A Case Study on Oxygen Evolution Reaction. *ACS Catal.* **2018**, *8*, 6617−6626.

(8) Xie, Y.-C.; Tang, Y.-Q. Spontaneous Monolayer Dispersion of Oxides and Salts onto Surfaces of Supports: Applications to Heterogeneous Catalysis. In *Advances in Catalysis*; Eley, D. D., Pines, H., Weisz, P. B., Eds.; Academic Press, 1990; Vol. *37*, pp 1−43.

(9) Moliner, M.; Gabay, J.; Kliewer, C.; Serna, P.; Corma, A. Trapping of Metal Atoms and Metal Clusters by Chabazite under Severe Redox Stress. *ACS Catal.* **2018**, *8*, 9520−9528.

(10) Prins, R. Hydrogen Spillover. Facts and Fiction. *Chem. Rev.* **2012**, *112*, 2714−2738.

(11) Nelson, N. C.; Nguyen, M.-T.; Glezakou, V.-A.; Rousseau, R.; Szanyi, J. Carboxyl intermediate formation via an in situ-generated metastable active site during water-gas shift catalysis. *Nat. Catal.* **2019**, *2*, 916−924.

(12) Wang, X.; Shi, H.; Kwak, J. H.; Szanyi, J. Mechanism of CO2 Hydrogenation on Pd/Al2O3 Catalysts: Kinetics and Transient DRIFTS-MS Studies. *ACS Catal.* **2015**, *5*, 6337−6349.

(13) Berger, R. J.; Pérez-Ramírez, J.; Kapteijn, F.; Moulijn, J. A. Catalyst performance testing: bed dilution revisited. *Chem. Eng. Sci.* **2002**, *57*, 4921−4932.

(14) Koros, R. M.; Nowak, E. J. A diagnostic test of the kinetic regime in a packed bed reactor. *Chem. Eng. Sci.* **1967**, *22*, 470.

(15) Nelson, N. C.; Chen, L.; Meira, D.; Kovarik, L.; Szanyi, J. In Situ Dispersion of Palladium on TiO_2 During Reverse Water−Gas Shift Reaction: Formation of Atomically Dispersed Palladium. *Angew. Chem., Int. Ed.* **2020**, *59*, 17657−17663.

(16) Schlatter, J.; Boudart, M. Hydrogenation of ethylene on supported platinum. *J. Catal.* **1972**, *24*, 482−492.

(17) Bianchi, D.; Lacroix, M.; Pajonk, G.; Teichner, S. Catalytic and infrared demonstrations of the effect of hydrogen spillover on a gel of silica. *J. Catal.* **1979**, *59*, 467−471.

(18) Bianchi, D.; Gardes, G. E. E.; Pajonk, G. M.; Teichner, S. J. Hydrogenation of ethylene on alumina after hydrogen spillover. *J. Catal.* **1975**, *38*, 135−146.

(19) Messou, D.; Bernardin, V.; Meunier, F.; Ordoño, M. B.; Urakawa, A.; Machado, B. F.; Collière, V.; Philippe, R.; Serp, P.; Le Berre, C. Origin of the synergistic effect between TiO2 crystalline phases in the Ni/TiO2-catalyzed CO2 methanation reaction. *J. Catal.* **2021**, *398*, 14−28.

(20) Baumgarten, E.; Lentes-Wagner, C.; Wagner, R. Hydrogen spillover through gas phase transport of hydrogen atoms. *J. Catal.* **1989**, *117*, 533−541.

(21) Cęckiewicz, S.; Delmon, B. Cooperative action of Ptγ-Al2O3 catalyst and γ-Al2O3 diluent in the hydrogenation of benzene. *J. Catal.* **1987**, *108*, 294−303.

(22) Antonucci, P.; van Truong, N.; Giordano, N.; Maggiore, R. Hydrogen spillover effects in the hydrogenation of benzene over Ptγ-Al_2O_3 catalysts. *J. Catal.* **1982**, *75*, 140−150.

(23) Sinfelt, J. H.; Lucchesi, P. J. Kinetic Evidence for the Migration of Reactive Intermediates in Surface Catalysis. *J. Am. Chem. Soc.* **1963**, *85*, 3365−3367.

(24) Sancier, K. Hydrogen migration on Alumina/Palladium catalysts for benzene hydrogenation. *J. Catal.* **1971**, *20*, 106−109.

(25) Nakamura, I.; Zhang, A.; Fan, Y.; Fujimoto, K. Interparticle migration of hydrogen on zeolite and their participation in the hydrogenation of adsorbed species and catalytic reaction. In *Studies in Surface Science and Catalysis*; Froment, G. F., Waugh, K. C., Eds.; Elsevier, 1997; Vol. *109*, pp 325−332.

(26) Spencer, M.; Burch, R.; Golunski, S. Comments on "hydrogen spillover through gas phase transport of hydrogen atoms". *J. Catal.* **1990**, *126*, 311−313.

(27) Garcia-Araez, N. Enthalpic and Entropic Effects on Hydrogen and OH Adsorption on Pt(111), Pt(100), and Pt(110) Electrodes As Evaluated by Gibbs Thermodynamics. *J. Phys. Chem. C* **2011**, *115*, 501−510.

(28) Briggs, D. Hydrogenation of ethylene on supported platinum. *J. Catal.* **1973**, *28*, 338.

(29) Wang, Y.; Wang, G.; van der Wal, L. I.; Cheng, K.; Zhang, Q.; de Jong, K. P.; Wang, Y. Visualizing Element Migration over Bifunctional Metal-Zeolite Catalysts and its Impact on Catalysis. *Angew. Chem., Int. Ed.* **2021**, *60*, 17735−17743.

(30) Nelson, N. C.; Szanyi, J. Heterolytic Hydrogen Activation: Understanding Support Effects in Water−Gas Shift, Hydrodeoxygenation, and CO Oxidation Catalysis. *ACS Catal.* **2020**, *10*, 5663−5671.

(31) Diebold, U. The surface science of titanium dioxide. *Surf. Sci. Rep.* **2003**, *48*, 53−229.

(32) Thomas, A. G.; Syres, K. L. Adsorption of organic molecules on rutile TiO2 and anatase TiO2 single crystal surfaces. *Chem. Soc. Rev.* **2012**, *41*, 4207−4217.

(33) Grinter, D. C.; Nicotra, M.; Thornton, G. Acetic Acid Adsorption on Anatase TiO2(101). *J. Phys. Chem. C* **2012**, *116*, 11643−11651.

(34) Khare, P.; Kumar, N.; Kumari, K. M.; Srivastava, S. S. Atmospheric formic and acetic acids: An overview. *Rev. Geophys.* **1999**, *37*, 227−248.

(35) Balajka, J.; Hines, M. A.; DeBenedetti, W. J. I.; Komora, M.; Pavelec, J.; Schmid, M.; Diebold, U. High-affinity adsorption leads to molecularly ordered interfaces on TiO2 in air and solution. *Science* **2018**, *361*, 786−789.

(36) Hasan, M. A.; Zaki, M. I.; Pasupulety, L. Oxide-catalyzed conversion of acetic acid into acetone: an FTIR spectroscopic investigation. *Appl. Catal., A* **2003**, *243*, 81−92.

(37) Pei, Z.-F.; Ponec, V. On the intermediates of the acetic acid reactions on oxides: an IR study. *Appl. Surf. Sci.* **1996**, *103*, 171−182.

(38) Rubasinghege, G.; Ogden, S.; Baltrusaitis, J.; Grassian, V. H. Heterogeneous Uptake and Adsorption of Gas-Phase Formic Acid on Oxide and Clay Particle Surfaces: The Roles of Surface Hydroxyl Groups and Adsorbed Water in Formic Acid Adsorption and the

https://doi.org/10.1021/acscatal.1c03133
ACS Catal. XXXX, XXX, XXX−XXX

Impact of Formic Acid Adsorption on Water Uptake. *J. Phys. Chem. A* **2013**, *117*, 11316−11327.
(39) Mattsson, A.; Österlund, L. Adsorption and Photoinduced Decomposition of Acetone and Acetic Acid on Anatase, Brookite, and Rutile TiO2 Nanoparticles. *J. Phys. Chem. C* **2010**, *114*, 14121−14132.
(40) Tabacchi, G.; Fabbiani, M.; Mino, L.; Martra, G.; Fois, E. The Case of Formic Acid on Anatase TiO_2(101): Where is the Acid Proton? *Angew. Chem., Int. Ed.* **2019**, *58*, 12431−12434.
(41) Sun, Z.; Kong, L.; Ding, X.; Du, C.; Zhao, X.; Chen, J.; Fu, H.; Yang, X.; Cheng, T. The effects of acetaldehyde, glyoxal and acetic acid on the heterogeneous reaction of nitrogen dioxide on gamma-alumina. *Phys. Chem. Chem. Phys.* **2016**, *18*, 9367−9376.
(42) Backes, M. J.; Lukaski, A. C.; Muggli, D. S. Active sites and effects of H2O and temperature on the photocatalytic oxidation of 13C-acetic acid on TiO2. *Appl. Catal., B* **2005**, *61*, 21−35.
(43) Deacon, G.; Phillips, R. J. Relationships between the carbon-oxygen stretching frequencies of carboxylato complexes and the type of carboxylate coordination. *Coord. Chem. Rev.* **1980**, *33*, 227−250.
(44) Tong, S. R.; Wu, L. Y.; Ge, M. F.; Wang, W. G.; Pu, Z. F. Heterogeneous chemistry of monocarboxylic acids on α-Al_2O_3 at different relative humidities. *Atmos. Chem. Phys.* **2010**, *10*, 7561−7574.
(45) Wang, X.; Hong, Y.; Shi, H.; Szanyi, J. Kinetic modeling and transient DRIFTS−MS studies of CO_2 methanation over Ru/Al_2O_3 catalysts. *J. Catal.* **2016**, *343*, 185−195.
(46) Wang, X.; Shi, H.; Szanyi, J. Controlling selectivities in CO2 reduction through mechanistic understanding. *Nat. Commun.* **2017**, *8*, 513.
(47) Leyva-Porras, C.; Toxqui-Teran, A.; Vega-Becerra, O.; Miki-Yoshida, M.; Rojas-Villalobos, M.; García-Guaderrama, M.; Aguilar-Martínez, J. A. Low-temperature synthesis and characterization of anatase TiO_2 nanoparticles by an acid assisted sol−gel method. *J. Alloys Compd.* **2015**, *647*, 627−636.
(48) Szanyi, J.; Kwak, J. H. Dissecting the steps of CO_2 reduction: 2. The interaction of CO and CO_2 with Pd/γ-Al_2O_3: an in situ FTIR study. *Phys. Chem. Chem. Phys.* **2014**, *16*, 15126−15138.
(49) Szanyi, J.; Kwak, J. H. Dissecting the steps of CO_2 reduction: 1. The interaction of CO and CO_2 with γ-Al_2O_3: an in situ FTIR study. *Phys. Chem. Chem. Phys.* **2014**, *16*, 15117−15125.
(50) Evans, H. E.; Weinberg, W. H. A comparison of the vibrational structures of ethanol, acetic acid, and acetaldehyde adsorbed on alumina. *J. Chem. Phys.* **1979**, *71*, 4789−4798.
(51) Manzhos, S.; Giorgi, G.; Yamashita, K. A Density Functional Tight Binding Study of Acetic Acid Adsorption on Crystalline and Amorphous Surfaces of Titania. *Molecules* **2015**, *20*, 3371−3388.
(52) Günnemann, C.; Haisch, C.; Fleisch, M.; Schneider, J.; Emeline, A. V.; Bahnemann, D. W. Insights into Different Photocatalytic Oxidation Activities of Anatase, Brookite, and Rutile Single-Crystal Facets. *ACS Catal.* **2019**, *9*, 1001−1012.
(53) Parkinson, G. S.; Novotny, Z.; Argentero, G.; Schmid, M.; Pavelec, J.; Kosak, R.; Blaha, P.; Diebold, U. Carbon monoxide-induced adatom sintering in a Pd−Fe_3O_4 model catalyst. *Nat. Mater.* **2013**, *12*, 724−728.
(54) Bliem, R.; van der Hoeven, J.; Zavodny, A.; Gamba, O.; Pavelec, J.; de Jongh, P. E.; Schmid, M.; Diebold, U.; Parkinson, G. S. An Atomic-Scale View of CO and H_2 Oxidation on a Pt/Fe_3O_4 Model Catalyst. *Angew. Chem., Int. Ed.* **2015**, *54*, 13999−14002.
(55) Nie, L.; Mei, D.; Xiong, H.; Peng, B.; Ren, Z.; Hernandez, X. I. P.; DeLaRiva, A.; Wang, M.; Engelhard, M. H.; Kovarik, L.; Datye, A. K.; Wang, Y. Activation of surface lattice oxygen in single-atom Pt/CeO2 for low-temperature CO oxidation. *Science* **2017**, *358*, 1419−1423.
(56) Jones, J.; Xiong, H.; DeLaRiva, A. T.; Peterson, E. J.; Pham, H.; Challa, S. R.; Qi, G.; Oh, S.; Wiebenga, M. H.; Pereira Hernandez, X. I.; Wang, Y.; Datye, A. K. Thermally stable single-atom platinum-on-ceria catalysts via atom trapping. *Science* **2016**, *353*, 150−154.
(57) Peterson, E. J.; DeLaRiva, A. T.; Lin, S.; Johnson, R. S.; Guo, H.; Miller, J. T.; Hun Kwak, J.; Peden, C. H. F.; Kiefer, B.; Allard, L. F.; Ribeiro, F. H.; Datye, A. K. Low-temperature carbon monoxide oxidation catalysed by regenerable atomically dispersed palladium on alumina. *Nat. Commun.* **2014**, *5*, 4885.
(58) Wettergren, K.; Schweinberger, F. F.; Deiana, D.; Ridge, C. J.; Crampton, A. S.; Rötzer, M. D.; Hansen, T. W.; Zhdanov, V. P.; Heiz, U.; Langhammer, C. High Sintering Resistance of Size-Selected Platinum Cluster Catalysts by Suppressed Ostwald Ripening. *Nano Lett.* **2014**, *14*, 5803−5809.
(59) Ouyang, R.; Liu, J.-X.; Li, W.-X. Atomistic Theory of Ostwald Ripening and Disintegration of Supported Metal Particles under Reaction Conditions. *J. Am. Chem. Soc.* **2013**, *135*, 1760−1771.
(60) Hansen, T. W.; DeLaRiva, A. T.; Challa, S. R.; Datye, A. K. Sintering of Catalytic Nanoparticles: Particle Migration or Ostwald Ripening? *Acc. Chem. Res.* **2013**, *46*, 1720−1730.
(61) Morgan, K.; Goguet, A.; Hardacre, C. Metal Redispersion Strategies for Recycling of Supported Metal Catalysts: A Perspective. *ACS Catal.* **2015**, *5*, 3430−3445.
(62) Suzuki, A.; Inada, Y.; Yamaguchi, A.; Chihara, T.; Yuasa, M.; Nomura, M.; Iwasawa, Y. Time Scale and Elementary Steps of CO-Induced Disintegration of Surface Rhodium Clusters. *Angew. Chem., Int. Ed.* **2003**, *42*, 4795−4799.

https://doi.org/10.1021/acscatal.1c03133
ACS Catal. XXXX, XXX, XXX−XXX